



Ameliorating Amyloid- β Fibrils Triggered Inflammation *via* Curcumin-Loaded Polymeric Nanoconstructs

Andrea Ameruso¹, Roberto Palomba¹, Anna Lisa Palange¹, Antonio Cervadoro¹, Aeju Lee², Daniele Di Mascolo^{1†} and Paolo Decuzzi^{1*†}

¹Laboratory of Nanotechnology for Precision Medicine, Fondazione Istituto Italiano di Tecnologia, Genoa, Italy,

²International Research Organization for Advanced Science and Technology (IROAST), Kumamoto University, Kumamoto, Kumamoto Prefecture, Japan

OPEN ACCESS

Edited by:

Paola Italiani,
Consiglio Nazionale Delle
Ricerche (CNR), Italy

Reviewed by:

Attilio Iemolo,
University of California,
San Diego, United States
Seyed Moein Moghimi,
Durham University,
United Kingdom

*Correspondence:

Paolo Decuzzi
paolo.decuzzi@iit.it

[†]These authors share
the senior authorship.

Specialty section:

This article was submitted
to Inflammation,
a section of the journal
Frontiers in Immunology

Received: 31 January 2017

Accepted: 11 October 2017

Published: 31 October 2017

Citation:

Ameruso A, Palomba R,
Palange AL, Cervadoro A, Lee A,
Di Mascolo D and Decuzzi P (2017)
Ameliorating Amyloid- β Fibrils
Triggered Inflammation *via*
Curcumin-Loaded Polymeric
Nanoconstructs.
Front. Immunol. 8:1411.
doi: 10.3389/fimmu.2017.01411

Inflammation is a common hallmark in several diseases, including atherosclerosis, cancer, obesity, and neurodegeneration. In Alzheimer's disease (AD), growing evidence directly correlates neuronal damage with inflammation of myeloid brain cells, such as microglia. Here, polymeric nanoparticles were engineered and characterized for the delivery of anti-inflammatory molecules to macrophages stimulated via direct incubation with amyloid- β fibers. 200 nm spherical polymeric nanoconstructs (SPNs) and 1,000 nm discoidal polymeric nanoconstructs (DPNs) were synthesized using poly(lactic-co-glycolic acid) (PLGA), polyethylene glycol (PEG), and lipid chains as building blocks. First, the internalization propensity in macrophages of both nanoparticles was assessed *via* cytofluorimetric and confocal microscopy analyses, demonstrating that SPNs are by far more rapidly taken up as compared to DPNs (99.6 ± 0.11 vs $14.4 \pm 0.06\%$, within 24 h). Then, Curcumin-loaded SPNs (Curc-SPNs) were realized by encapsulating Curcumin, a natural anti-inflammatory molecule, within the PLGA core of SPNs. Finally, Curc-SPNs were shown to diminish up to 6.5-fold the production of pro-inflammatory cytokines—IL-1 β ; IL-6, and TNF- α —in macrophages stimulated *via* amyloid- β fibers. Although more sophisticated *in vitro* models and systematic analyses on the blood-brain barrier permeability are critically needed, these findings hold potential in the development of nanoparticles for modulating inflammation in AD.

Keywords: nanoparticle, inflammation, systemic delivery, neurodegenerative diseases, macrophage activation

INTRODUCTION

Inflammation is a defense response to external pathogens and other insults which is precisely orchestrated by our immune system. However, under certain conditions, inflammatory processes could become detrimental and lead to severe pathological states (1). This is the case of atherosclerosis where monocyte infiltration into the vessel walls and maturation into macrophages are key events in the formation and progression of vascular plaques (2). Inflammation and immune cells play a role in cancer too where tumor-associated macrophages could protect and sustain the growth of malignant cells (3). Moreover, in obesity, macrophage infiltration in adipose tissue causes local and systemic inflammation eventually leading to insulin resistance (4). Similarly, in Alzheimer's

disease (AD), mounting evidence indicates that macrophages of the central nervous system—microglia—contribute to the onset of the disease and sustain neurotoxicity (5, 6). While under physiological conditions, microglia serve as immune surveilling cells, upon injury or immune stimuli activation, microglia secrete pro-inflammatory cytokines that are eventually responsible of neuronal death. Following the amyloid cascade hypothesis, microglia activation is triggered in Alzheimer's disease by amyloid- β plaques (A β s), resulting from the extracellular accumulation of amyloid- β peptides, and neurofibrillary tangles, deriving from the clustering of the microtubule-associated protein tau. Over a sufficiently long time, this is responsible of chronic brain inflammation and production of pro-inflammatory cytokines, such as IL-1 β , IL-6, TNF- α , and many others (7).

Nanomedicines are slowly but surely accessing clinical practice for the treatment of deadly diseases, so far primarily involving cancer and cardiovascular (8, 9). Over 40 liposomal and polymeric nanoparticles are currently undergoing clinical investigation and a few nano-based products are already routinely used by oncologists (liposomal doxorubicin and albumin-bound paclitaxel). Over single therapeutic agents, nanomedicines can carry and deliver multiple drug molecules to diseased sites following specific release profiles; protect the payload from enzymatic degradations and enhance bioavailability; provide useful information at the cellular and tissue scales for designing patient-specific therapeutic interventions. Furthermore, the size, shape, surface properties, and mechanical stiffness of nanomedicines can be often precisely tailored during the fabrication process to enhance accumulation at the biological target and mitigate adverse effects deriving by off-targeting (10–15). Importantly, properly designed nanoparticles can be rapidly taken up by activated macrophages residing in different vascular districts and tissues. This gives the opportunity of efficiently using nanoparticles to deliver directly into activated macrophages anti-inflammatory agents, possibly modulating both locally and systemically the inflammatory state. The authors and other groups have loaded nanoparticles with a variety of anti-inflammatory molecules, starting with the natural, broad-spectrum molecule Curcumin and moving to drugs with more specific sub-cellular targets as diclofenac (16–18). Note that both Curcumin and diclofenac are hydrophobic, exhibit a poor bioavailability and their specific, systemic administration can be largely improved *via* encapsulation into nanoparticles.

This work aims at selecting nanoparticles for the specific delivery of Curcumin to macrophages which have been activated by incubation with amyloid- β fibrils. First, two different nanoparticle configurations were considered, namely spherical polymeric nanoconstruct (SPNs) with a characteristic size of about 200 nm and discoidal polymeric nanoconstructs (DPNs) with a diameter of 1,000 nm and height of 400 nm (15, 17). Both nanoparticles were realized with biodegradable and biocompatible polymers—poly(lactic-*co*-glycolic acid) (PLGA), polyethylene glycol (PEG)—mixed with lipid chains. Then, the most effective configuration was selected based on macrophage internalization assays involving cytofluorimetric and confocal microscopy analyses. Finally, the selected configuration was loaded with Curcumin and delivered to macrophages, in the

presence of amyloid- β fibrils, for assessing IL-1 β ; IL-6 and TNF- α production.

MATERIALS AND METHODS

Materials

Poly(lactic-*co*-glycolic acid) (50:50, Carboxy-terminated, MW 38,000–54,000 Da) was purchased from Sigma Aldrich (St. Louis, MO, USA). 1,2-dipalmitoyl-sn-glycero-3-phosphocholine (DPPC) and 1,2-distearoyl-sn-glycero-3-phosphoethanolamine-N-[Carboxy(Polyethylene Glycol)-2000] (DSPE-PEG) were obtained from Avanti Polar Lipids (Alabaster, Alabama). Curcumin (95% total curcuminoid content) was purchased from Alfa Aesar. Chloroform, Acetonitrile and other solvents were obtained from Sigma Aldrich.

Nanoparticle Synthesis and Characterization

Spherical polymeric nanoconstructs (SPNs) were synthesized by employing an emulsion/solvent evaporation technique (17). DSPE-PEG was dissolved in a 4% ethanol solution to a final volume of 3 ml to obtain the aqueous phase, whereas 1 mg of PLGA and an appropriate quantity of DPPC were dissolved in chloroform to create the oil phase. A v/v ratio of 6:1 between the aqueous and organic phase, a lipids/polymer w/w ratio of 20% and a DPPC/DSPE-PEG molar ratio of 7.5:2.5 were used. Then, the oil phase was added in a dropwise manner to the aqueous solution under ultrasonication at 60% amplitude (Q125 sonicator, Q-Sonica). The resulting emulsion was then gently stirred at room temperature and in a reduced pressure environment for 4 h to allow solvent evaporation. Finally, nanoparticles were washed with water by centrifugation using Amicon Ultra-4, Centrifugal Filter 10,000 Da (Millipore) at 3,500 rpm for 8 min for three times to remove any possible debris obtained in the synthesis process. SPN size and surface zeta potential were estimated by dynamic light scattering (DLS) (Malvern Zetasizer, ZEN 3600). To this end, nanoparticles solution was centrifuged at 12,000 rpm for 20 min and the pellet was resuspended in 1 ml of Milli-Q water; then, 20 μ l were diluted in 1 ml of Milli-Q water and the resulting solution was transferred into a folded capillary cell (Malvern). The Smoluchowski model was used to calculate zeta potential values. For scanning electron microscopy (SEM) analysis, the SPN solution was dropped directly onto a polished silicon wafer. After drying, samples were sputter-coated with platinum prior to imaging, to enhance polymer contrast. The stability of the nanoparticles was evaluated over a period of 9 days. Nanoparticles were suspended in 1 ml of Milli-Q water and kept at 37°C for the whole time span. At various time points (namely at days 1, 2, 3, 5, and 9), a DLS analysis on each sample was performed as described above. For each characterization study, the number of analyzed samples was 3.

Discoidal polymeric nanoconstructs were synthesized by employing a top-down fabrication process described in details in our previous works (14, 15). Briefly, this fabrication approach involves the use of electron beam lithography (EBL) to fabricate a silicon master template presenting an array of cylindrical holes

with a fixed diameter (1,000 nm) and height (400 nm). This pattern is then replicated into PDMS and subsequently PVA templates, by using soft lithography techniques. Once the holes of the sacrificial template (PVA) are filled with the polymeric mixture composed by PLGA and PEG, the PVA is dissolved in water to collect the resulting particles. To perform internalization experiments, lipid Rhodamine was added to the polymeric mixture composing DPNs. DPN physical chemical characterization was performed through Multisizer (Beckman Coulter) to calculate DPN concentration and size distribution profile, and DLS to estimate the zeta potential. The samples for transmission electron microscopy (TEM) were prepared by the drop casting method over copper grid. The samples were negatively stained for 10 min with 2% (w/v) uranyl acetate aqueous solution, and then washed twice with distilled water and dried before imaging. The stability of the DPNs was evaluated as described above for the SPNs ($n = 3$).

Cell Cultures

Raw 264.7 cells were purchased from the American Type Culture Collection (ATCC, Rockville, MD, USA) and maintained in Dulbecco's Modified Eagle's Medium high-glucose (DMEM) (Euroclone) supplemented with 10% fetal bovine serum (ATCC) and 1% penicillin/streptomycin. Cells were grown at 37°C in an 80% humidified atmosphere of 5% CO₂.

Internalization Experiments

2×10^5 RAW 264.7 cells were seeded into a 12 well plate. Cells were treated with SPNs (1.5 µg/ml), Fluoresbrite® Carboxyl NYO Carboxylate Microspheres 0.20 µm (Polyscience) (30 Particles per cell), and DPNs (10 particles per cell). 24 h later cells were harvested in phenol red free DMEM (Lonza) and analyzed by flow cytometry using BD FACS Aria (Beckton Dickinson). 2×10^5 events per sample were analyzed, and experiments were run in triplicate. For microscopy analyses, 1×10^4 RAW 264.7 cells were seeded into a Lab-Tek II Chambered Coverglass (Thermo Fisher). Cells were treated following the same condition described above. Images were acquired using A1 + Nikon confocal microscope system (Nikon). Statistic was performed analyzing four images per each group and performed in triplicate.

Drug Loading (DL) and Release

Curcumin-loaded SPNs (Curc-SPNs) were synthesized by employing the same emulsion/solvent evaporation technique described above. Simply, the 200 µg of Curcumin was dissolved in chloroform and added to the oil phase per each milligram of PLGA. To estimate loading and encapsulation efficiency (EE), SPNs were resuspended in 1 ml of water and freeze-dried. After lyophilization, a known amount of particles was dissolved in acetonitrile to free the entrapped drug. The absorbance of Curcumin at 430 nm, with a baseline wavelength of 650 nm, was measured and used to calculate the amount of molecule. Each sample was evaluated in triplicate. Loading efficiency was expressed as the weight percentage of drug mass with respect to the total mass of the nanoparticles, whereas EE was expressed as the weight percentage of entrapped drug mass as compared

to the initial drug input. The *in vitro* release of Curcumin was evaluated under physiological conditions in PBS at 37°C and pH 7.4 up to 72 h. 200 µl of nanoparticle solution at 10 µM Curcumin were transferred into Slide-A-Lyzer MINI dialysis cups with a molecular cutoff of 10 kDa (Thermo Scientific, Rockford, IL, USA) and dialyzed against 4 l of PBS. At each time point, three replicates were retrieved and analyzed. Quantification of the amount of drug released was obtained through a spectrophotometric measurement, using a method akin to the one employed in assessing the loading efficiency. The content of each cup was collected and centrifuged at 12,000 rpm for 20 min, and the resulting pellet of nanoparticles was dissolved in acetonitrile. Then, for each sample, the absorbance at 430 nm with a baseline wavelength of 650 nm was measured. Results for each time point are expressed as a percentage with respect to the initial time point.

In Vitro Production of Amyloid-β Fibrils

Amyloid-β (Aβ) peptides (Aβ 1–42) (MW 4415.26, Sigma Aldrich) were dissolved by briefly vortexing in a 0.02% ammonia solution at a concentration of 1 mM at 4°C and stored at –80°C. Formation of Aβ fibrils was obtained through a polymerization reaction conducted as described by Ono and Hasegawa: Aβ peptides were dissolved in 50 mM phosphate buffer (pH 7.4, 100 mM NaCl) to a final concentration of 25 µM and to a final volume of 950 µl and incubated for 6 and 16 h at 37°C. The reaction was stopped by storing the samples at 4°C. Aβ fibrils were visualized *via* TEM. 4 µl of fibril solution were cast on a carbon-coated copper grid and positively stained for 10 min with a 2% (w/v) uranyl acetate aqueous solution. Samples were then washed with distilled water and dried before imaging.

Cell Viability Assay

Dead Cell Apoptosis Kit with Annexin V FITC and PI (ThermoFisher) was used to initially detect any apoptotic effect of PLGA, as main constituent of our particles, both SPNs and DPNs. Cells (2×10^5) were seeded and, after reaching confluency, were treated with empty nanoparticles, at three different concentrations, namely 0.05, 1.5, and 15 µg/ml of PLGA. After 12 h, cells were detached from the plates and stained using the aforementioned kit. Then FACS analyses were performed. An MTT (3-(4,5-Dimethylthiazol-2-yl)-2,5-Diphenyltetrazolium Bromide) proliferation assay (Sigma Aldrich) was used to evaluate the cytotoxicity of free Curcumin, empty nanoparticles, and Curcumin-loaded nanoparticles. Cells were seeded at a density of 5×10^3 cells per well in 96 well plates and cultured for 24 h. Free Curcumin was suspended in DMSO and diluted to various concentrations with complete cell media. DMSO was always kept at a final concentration below 0.1% v/v. Empty SPNs and Curcumin-SPNs were resuspended in complete media at various concentrations. These solutions were used to treat cells. After 24 h, the medium was removed and the MTT working solution was added according to the manufacturer's instructions. After 4 h, medium was removed and DMSO was added to each well to solubilize the purple precipitates. Upon complete solubilization, the absorbance at 570 nm was measured for each sample. In all groups, five replicates were analyzed per each of the used

concentration. Data are expressed as the percentage of viable cells with respect to controls.

Real-time RT-PCR

Raw 264.7 macrophages were seeded at a density of 2×10^5 cells/well in 6-well plates, containing 2 ml of culture media. Cells were pre-treated for 5 h with 10 μ M free Curcumin or Curc-SPNs and then exposed to 2 μ M A β fibrils and 100 ng/ml LPS (Sigma Aldrich). Cells were also exposed to empty SPNs, A β fibrils and LPS without previous treatment with Curc-SPNs. After 6 h, total RNA was extracted using RNeasy Plus Mini Kit (Qiagen) according to the manufacturer's instructions and quantified using Nanodrop 2000 UV-Vis Spectrophotometer (Thermo Scientific). Real Time RT-PCR were carried out using a Power SYBR Green RNA-to-CT 1-Step Kit (Applied Biosystems). The reactions were performed in a final volume of 20 μ l of the following reaction mixture: 2X Power SYBR Green RT-PCR Mix, 200 nM respective primer pairs, 125X RT Enzyme Mix, 100 ng of RNA template for retrotranscription and amplification of TNF- α , IL-1 β , or IL-6 gene product. GAPDH was used as housekeeping gene. Oligonucleotide primer pairs were as follows: for GAPDH, 5'-GAACATCATCCCTGCATCCA-3' and 5'-CCAGTGAGCTTCCCGTTCA-3'; for TNF- α , 5'-GGTG CCTATGTCTCAGCCTCTT-3' and 5'-GCCATAGAAGTGTATG AGAGGGAG-3'; for IL-1 β , 5'-TGGACCTTCCAGGATGAGGA CA-3' and 5'-GTTTCATCTCGGAGCCTGTAGTG-3'; for IL-6, 5'-TACCACTTACAAGTCGGAGGC-3' and 5'-CTGCAAGTG CATCATCGTTGTTC-3'. The fold change in gene expression was evaluated by $\Delta\Delta^{\text{Ct}}$ method, relative to the control. All experimental groups were tested in triplicate.

Statistical Analysis

Statistical analysis of significance was performed using ANOVA, after that equal-variance assumption was confirmed, using the robust Brown–Forsythe Levene-type test for homogeneity of variance. Multiple comparisons were performed using, as *post hoc* test, the Tukey's honestly significant difference (HSD) test. Comparisons with a *p*-value lower or equal to 0.05 was considered statistically significant different with respect to control. Data are presented as mean \pm SD.

RESULTS

Synthesis and Physico-Chemical Characterization of Spherical and DPNs

Spherical Polymeric Nanoconstructs (SPNs) were synthesized *via* an emulsion/solvent evaporation technique, as detailed in the Section "Materials and Methods" and in previous reports by the authors and other scientists (16, 17, 19). As schematically depicted in **Figure 1A**, SPNs exhibit a hydrophobic polymeric core made out of PLGA which is stabilized externally by a lipid monolayer comprising a mixture of dipalmitoyl-sn-glycero-3-phosphocholine (DPPC) and 1,2-distearoyl-sn-glycero-3-phosphoethanolamine-*N*-[amino(polyethylene glycol)-2000] with a carboxylic termination (DSPE-PEG-COOH). Following synthesis, SPNs were characterized for their physico-chemical properties. Specifically, SPN geometry (size and shape) was

analyzed *via* DLS and SEM. The SPN hydrodynamic size in de-ionized (DI) water resulted of 184.19 ± 15.06 nm, with a polydispersity index (PDI) of 0.115 ± 0.036 , based on DLS measurements (**Figure 1B**). The monodisperse population of SPNs is confirmed by the moderate PDI and the SEM image in **Figure 1C**. The ζ -potential of SPNs was of -43.18 ± 9.23 mV, documenting the presence of negative surface charges associated with the carboxylic termination of the DSPE-PEG-COOH chains. The colloidal stability of SPNs was also assessed by measuring longitudinally, over a period of 9 days, both the hydrodynamic size and PDI. The resulting data (**Figure 1D**) document a remarkable stability of SPNs with a negligible size and PDI variation over the whole period.

Discoidal polymeric nanoconstructs were synthesized *via* a top-down fabrication approach combining lithographic techniques, template replications and polymer mixture loading, as previously described by the authors (14, 15). As shown in **Figure 1E**, DPNs appear as circular disks resulting from cross linking PLGA and poly(ethylene glycol) diacrylate (PEG-DA) chains. Following synthesis, DPNs were characterized for their physico-chemical properties. Specifically, DPN geometry (size and shape) was analyzed *via* Multisizer characterization and TEM. Size assessment of DPNs, measured in DI water *via* Multisizer, returned an average size of 787 ± 27 nm (**Figure 1F**). Given the non-sphericity of DPNs, their size spectrum cannot present a single, sharp peak as for SPNs in **Figure 1B**. The TEM image in **Figure 1G** confirms the discoidal shape with a diameter of $\sim 1,000$ nm and a height of ~ 400 nm. The ζ -potential of DPNs was around -19.9 ± 4.56 mV, resulting from the balance between the neutral charge of the PEG chains and the negative surface charge associated with the carboxylic termination on the PLGA chains. The colloidal stability of DPNs was also assessed by measuring longitudinally, over a period of 9 days, the average size *via* Multisizer. The data reported in **Figure 1H** document a remarkable stability over time even for this second nanopatform.

Analysis of Macrophage Interaction with SPNs and DPNs

Cytofluorimetric analysis was performed in order to assess SPN and DPN internalization into professional phagocytic cells. The same volume ($\sim 1 \times 10^6 \mu\text{m}^3$) of polymeric particles was used. Specifically, SPNs (1.5 $\mu\text{g/ml}$), DPNs (10 particles per cells), and 200 nm carboxylated polystyrene particles (P200) (30 particles per cells) were incubated with Raw 264.7 cells up to 24 h. At 24 h, the percentage of RAW 264.7 cells associated with particles was $99.6 \pm 0.11\%$ for SPNs, $84.9 \pm 0.40\%$ for P200, and $14.4 \pm 0.06\%$ for DPNs (**Figure 2A**). This trend was also confirmed *via* confocal microscopy analyses. **Figure 2B** shows that 100% of RAW 264.7 cells within a region of interest resulted to be positive to SPNs and P200, while only $25.3 \pm 6.63\%$ of macrophages turned to be associated with DPNs. The panel of **Figure 2C** shows representative microscopy images of RAW 264.7 cells 24-h post incubation with SPNs, P200 and DPNs. In **Figure 2C**, nuclei and actin filaments were stained in blue and green, respectively, whereas nanoparticles appeared as red dots.

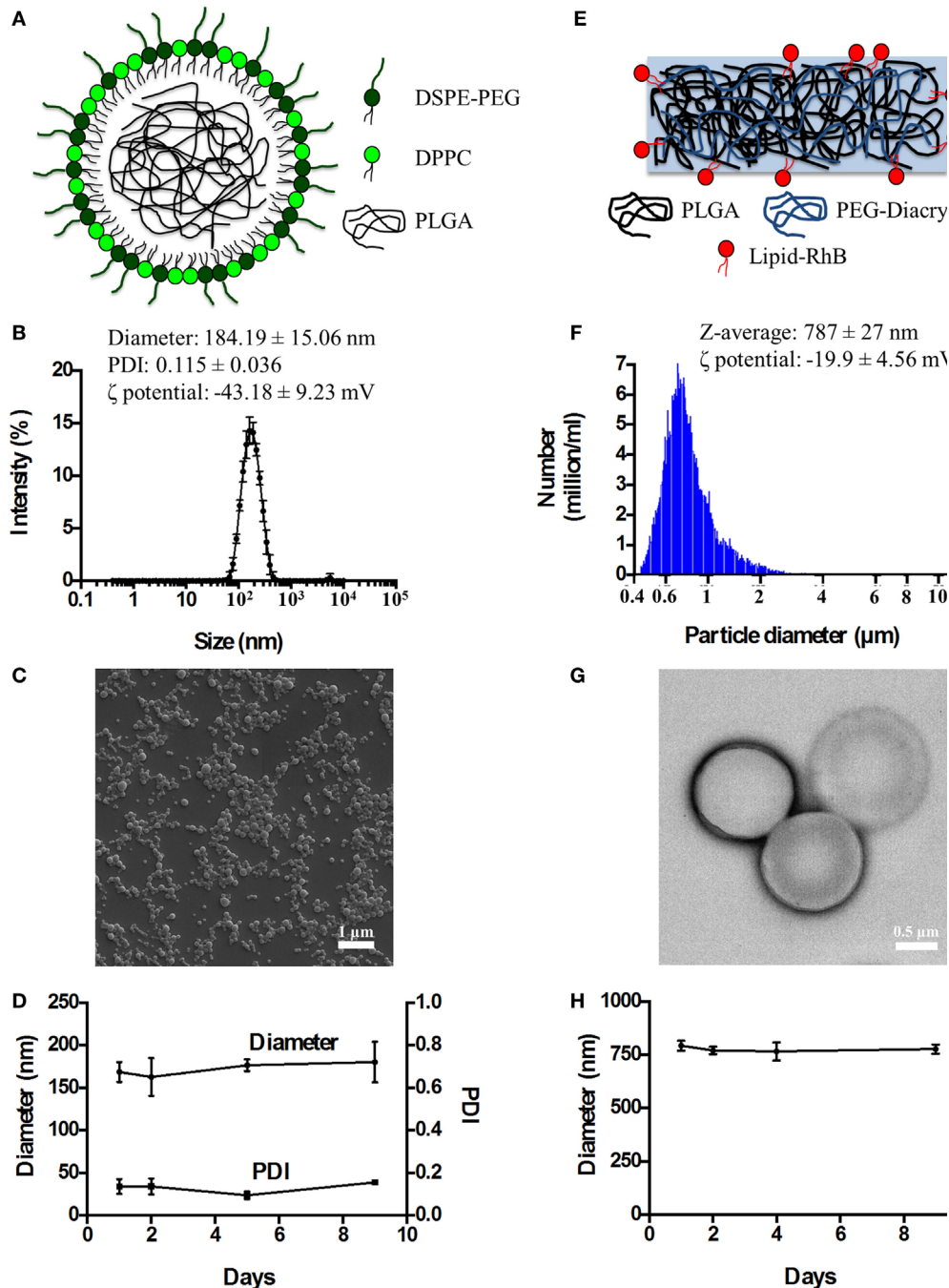
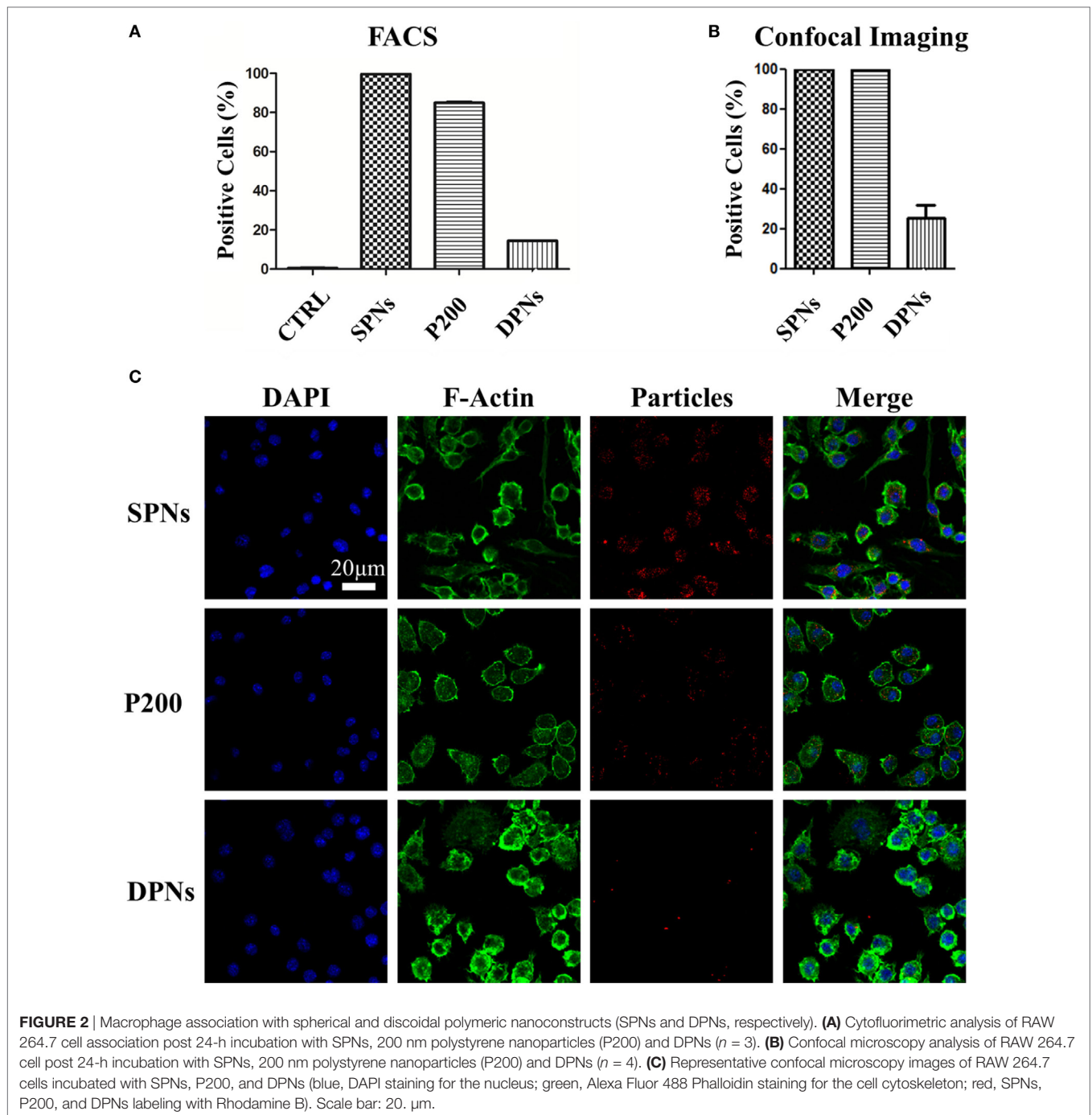


FIGURE 1 | The physico-chemical characterization of spherical and discoidal polymeric nanoconstructs. **(A)** Schematic representation of SPNs synthesized via emulsion/solvent evaporation method comprising a hydrophobic [poly(lactic-co-glycolic acid) (PLGA)] core stabilized by an external lipid monolayer (a mixture of DPPC and DSPE-PEG-COOH). **(B)** Size distribution of SPNs via dynamic light scattering analysis ($n = 3$). **(C)** Scanning electron microscopy image of SPNs. **(D)** Colloidal stability of SPNs in de-ionized (DI) water ($n = 3$). **(E)** Schematic representation of DPNs synthesized via a top-down approach and resulting by the crosslinking of PLGA and poly(ethylene glycol) diacrylate (PEG-DA) chains. **(F)** Size distribution of DPNs via Multisizer analysis ($n = 3$). **(G)** Transmission electron microscopy image of DPNs. **(H)** Colloidal stability of DPNs in DI water ($n = 3$).

It is clearly confirmed the large difference in cell uptake between the spherical nanoparticles, SPNs and P200, and the discoidal nanoconstructs DPNs. Also, multiple SPNs and P200 are associated with the same cell.

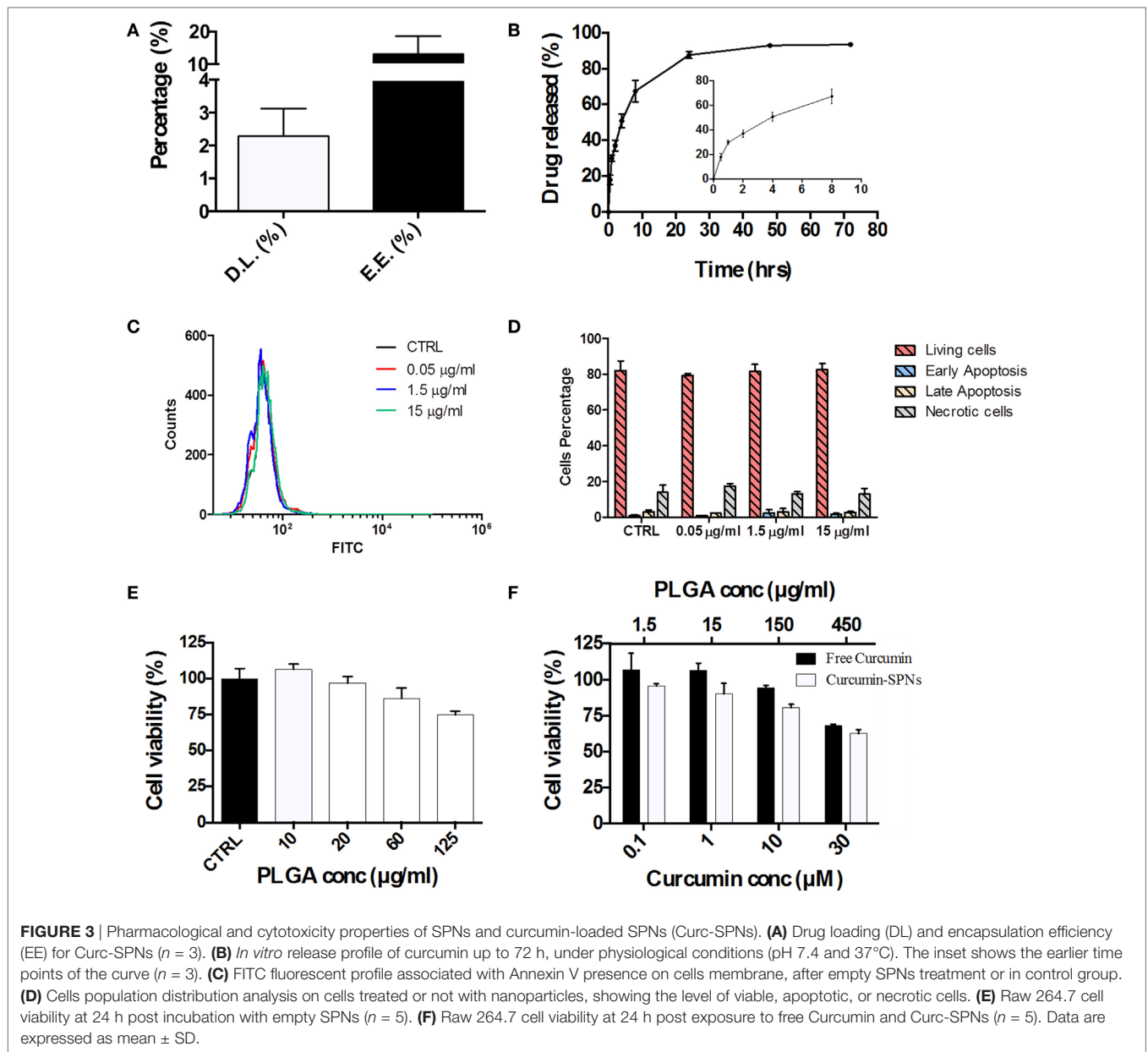
Pharmacological and Cytotoxicity Properties of SPNs

Based on the cell internalization results, SPNs were selected to be loaded with the natural, anti-inflammatory compound



Curcumin. Given the hydrophobicity profile of this molecule, Curcumin was directly entrapped within the hydrophobic PLGA core of SPNs. Curc-SPNs present a hydrodynamic size of 193.4 ± 6.9 nm and a zeta potential of -43.8 ± 4.56 mV. The pharmacological properties of Curc-SPNs were characterized by quantifying DL and release, and cytotoxicity on RAW 264.7 macrophages. To this end, Curcumin EE and loading were assessed *via* spectrophotometric analysis. DL was calculated as the percentage in weight of loaded Curcumin compared to the total nanoparticle mass; whereas the EE was determined

as the percentage of loaded Curcumin over the initial input amount of Curcumin. Data returned a DL of $2.31\% \pm 0.84$ and an EE of $13.23\% \pm 5.41$, as graphically reported in **Figure 3A**. The release profile of Curcumin was determined over a period of 72 h, under physiological conditions ($\text{pH} = 7.4$ and 37°C). As documented by the plot of **Figure 3B**, 50% of Curcumin was released within the first 6 h (see inset of **Figure 3B**), whereas the remaining 50% of anti-inflammatory molecules was slowly released within the following 66 h. The effect of SPNs in generating apoptosis, if any, was tested. **Figure 3C** shows the FITC



intensity profiles, indicating the level of apoptosis, for all the experimental conditions used. There is no difference among cells untreated or treated with different empty SPNs concentrations, not even at a concentration three times higher than the one used for internalization experiments. **Figure 3D** shows more insights on the cell populations analyzed, showing the level of living cells, necrotic cells, or cells in early or late apoptosis. Also in this case, cells distribution in these subgroups is similar, despite the treatment used. Taken together, these results prove that our SPNs do not induce apoptosis, at least in the time frame and in the conditions used for the subsequent Curc-SPNs efficacy experiments. Finally, the cytotoxicity on Raw 264.7 cells of empty SPNs, free Curcumin, and Curc-SPNs was quantified at 24 h, using a MTT cell proliferation assay.

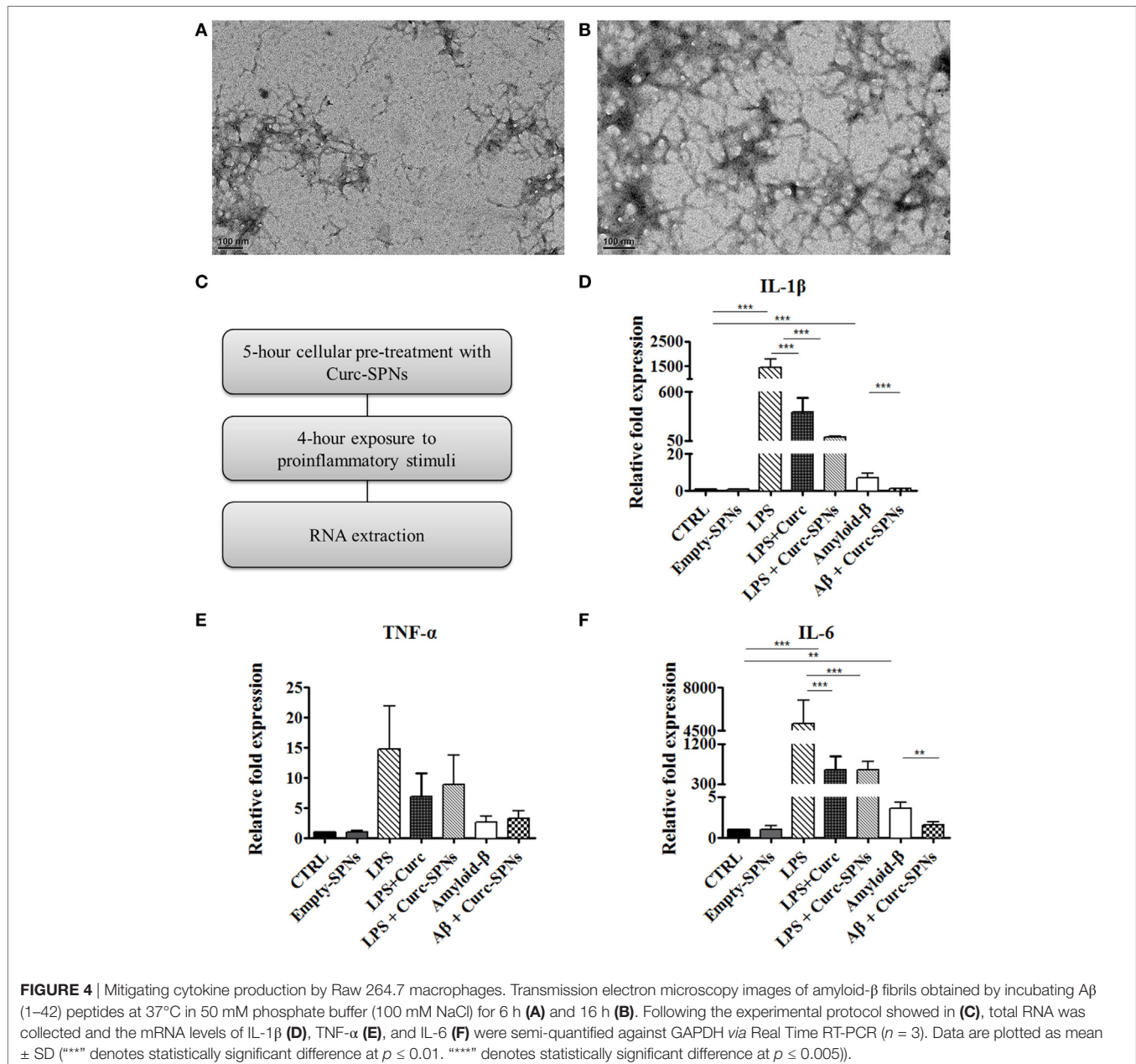
Figure 3E shows the cell viability of Raw 264.7 incubated with empty SPNs. No significant toxicity of SPNs was detected up to more than 20 $\mu\text{g/ml}$ of polymer. For larger concentrations, cell viability slightly reduces reaching an average value above 75% for 125 $\mu\text{g/ml}$ of polymer, although without any significant difference with control. This is very important as this is the polymer concentration representing the amount of polymer of 10 μM Curc-SPNs. **Figure 3F** directly compares the cytotoxicity potential of free Curcumin and Curc-SPNs. No significant toxicity was detected up to 10 μM of Curcumin, whereas, for larger concentrations, cell viability reduced steadily in a concentration dependent fashion. Also, Curc-SPNs and free Curcumin returned comparable cytotoxicity activities on RAW 264.7.

Anti-inflammatory Efficacy of Curc-SPNs

Inflammation was induced in RAW 264.7 cells by two different methods: incubation with A β fibrils and incubation with LPS, as positive control. Fibrils were obtained through spontaneous polymerization by incubating A β (1–42) peptides at 37°C for 6 or 16 h. Both procedures yielded fibrillar structures of 6–9 nm in diameter and more than 200 nm in length, as shown in **Figures 4A,B**. Since no dramatic differences were observed between the two polymerization protocols, the 6-h polymerization was selected for all subsequent experiments.

For assessing the anti-inflammatory potential of Curc-SPNs, Raw 264.7 macrophages were pre-incubated for 5 h with Curc-SPNs (10 μ M) and then exposed to an inflammatory stimulus

for 6 h (2 μ M of fibrillar A β or 100 ng/ml of LPS, as a positive control) (**Figure 4C**). The inflammatory response was assessed by measuring the levels of relevant pro-inflammatory cytokines, namely IL-1 β , IL-6, and TNF- α , *via* RT-PCR (**Figures 4D–F**). No changes in gene expression were observed when treating cells with an equivalent dose empty SPNs, this additional control prove the presence of negligible levels of endotoxins, if any. **Figures 4D–F** show the relative fold expression levels for the three cytokines in six different experimental groups: the control group (CTRL)—cells were neither treated with SPNs not exposed to pro-inflammatory stimuli; the empty-SPNs group—cells were exposed to empty SPNs to verify the possible pro-inflammatory potential of nanoparticles; the LPS group—cells were exposed



for 6 h to LPS without any SPN pre-treatment; the LPS + free Curcumin group—cells were pre-treated with 10 μ M Curcumin and then stimulated by LPS; the LPS + Curc-SPNs group—cells were prior incubated with Curc-SPNs for 5 h and subsequently exposed to LPS for 6 h; the Amyloid- β group—cells were exposed for 6 h to fibrillar A β without any SPN pre-treatment; the A β + Curc-SPNs group—cells were prior incubated with Curc-SPNs for 5 h, and subsequently exposed to fibrillar A β for 6 h. **Figure 4D** shows that the cellular production of IL-1 β is dramatically inhibited by a 5-h pre-treatment with Curc-SPNs. The relative cytokine expression reduces by \sim 15 times with respect to the case of LPS (from $1,439.67 \pm 340.77$ for LPS to 96.47 ± 4.33 for LPS + Curc-SPNs) and by \sim 6.5 times compared to fibrillar A β stimulation (from 7.21 ± 2.08 for Amyloid- β to 1.1 ± 0.17 for A β + Curc-SPNs). Free Curcumin treatment was also able to reduce IL-1 β , although at a more modest level (369.28 ± 164.33) compared LPS stimulation. Similar observations can be drawn from **Figure 4E** for IL-6. The relative cytokine expression reduces by \sim 8 times when compared to the case of LPS stimulation (from $5,053.44 \pm 1,928.49$ for LPS to 618.19 ± 189.49 for LPS + Curc-SPNs) and by \sim 2.3 times to the case of fibrillar A β stimulation (from 3.61 ± 0.78 for Amyloid- β to 1.57 ± 0.41 for A β + Curc-SPNs). In this respect, free curcumin showed a very similar behavior (620.123 ± 302.51). Although the same general trend can also be depicted in **Figure 4F**, no statistically significant variations in the expression of TNF- α was observed for LPS and fibrillar A β stimulations, both in the case of free Curcumin and Curc-SPNs pre-treatment. This could be due to the specific phenotype of RAW 264.7 cells, stimulation times, and concentrations of pro-inflammatory stimuli.

DISCUSSION

Inflammation is relevant in the onset and progression of several diseases, including cancer, cardiovascular, metabolic, and neurodegenerative. Until the harmful stimulus persists, the inflammatory machinery evolves into a chronic process, reinforcing and turning itself into a injurious course, worsening the condition at the damaged site. Macrophages, phagocytic cells of myeloid origin, are key players in this kind of chronic inflammation (20). They can be found in every body tissue, assuming different phenotypes and roles: they can be differentiated into several kinds of cells, including microglia, Kupffer cells, and more. In this chronic insult scenario, macrophages proceed in their accumulation resulting in their continuous activation largely responsible for inducing damage. AD pathology is also characterized by an inflammatory response, which is primarily driven by the brain-resident macrophages, i.e., microglia, most likely toward A β plaques, exacerbating the pathology of the disease, escalating with its progression (5, 6). Microglia surrounds and is intimately associated with A β plaques, which in turn leads to the production of inflammatory cytokines and chemokines *in vitro* (21–28). Furthermore, a panoply of typical inflammatory mediators can be detected both in *in vivo* models and in brains or CSF from AD patients, including TNF- α , IL-1 β , IL-6, GM-CSF, IL-12, and IL-23 (29–32). Even though microglia have the capacity to phagocytose A β , it is also true that the

inefficient clearance of amyloid plaques is a major pathogenic factor in AD (33). Based on this, it is of crucial importance to try to modulate macrophages phenotype, inducing a regression in their pro-inflammatory activity. In this work, two different nanoconstructs—SPNs and DPNs—were presented and characterized with the objective of selecting the best nanopatform for tempering inflammation in AD. Recently, different studies are trying to better understand and evaluate the interaction of nanoparticles and immune system cells. Small spherical nanoparticles, below 200 nm in diameter, seem to be more easily internalized by dendritic cells (34). Nonetheless, also nanoparticles' softness and deformability plays a very important role in this process. In fact, both *in vitro* and *in vivo* data showed that harder particles are more prone to be phagocytized, as well as to be removed from blood circulation (e.g., through spleen filtration) (15, 35). Moreover, the comparison between SPNs and DPNs was not only instrumental to choose the best platform to be used, but also increased the knowledge of this special interaction, so useful for any nano-based drug delivery system. Cytofluorimetric analysis revealed that, at 24 h post incubation, 99.6% of RAW 264.7 cells were associated with SPNs as opposed to only 14.4% for DPNs. This behavior was also confirmed *via* confocal microscopy analysis. Notably, SPNs worked even better than polystyrene particles, chosen as a positive control since they are easily uptaken by phagocytic cells, as well documented in the literature (36, 37). The ability of SPNs to be internalized and modulate macrophages activity was already demonstrated by the authors (38–40). Therefore, these new data provide additional information, unequivocally suggesting that spherical nanoparticles are far better candidates for delivering anti-inflammatory drugs directly into macrophages compared to discoidal nanoconstructs. Consequently, SPNs were selected as the delivery platform and were loaded with Curcumin, a natural anti-inflammatory molecule, in order to deliver their payload inside target cells. Curcumin (diferuloylmethane) is a polyphenol that represents the major curcuminoid extracted from the *Curcuma longa* plant, which is extensively used for its anti-inflammatory, antioxidant, analgesic, antiseptic, and anticancer activity (41). In particular, its anti-inflammatory effect, mostly due to the inhibition of NF- κ B transcription factor, makes Curcumin a highly desirable candidate as a therapeutic agent in several inflammation-based pathologies (42). However, Curcumin has a poor bioavailability of its hydrophobicity. For instance, in pre-clinical studies on rats, an oral dose of 500 mg/kg resulted in a peak plasma concentration of only 1.8 ng/ml (43). In a phase II clinical trial, 25 patients with pancreatic cancer were administered daily with 8 g of Curcumin leading to a maximum plasma level concentration of only 41 ng/ml (44, 45). In this manuscript, RAW 264.7 cells were exposed to amyloid- β fibrils and LPS, two potent pro-inflammatory stimuli, in order to replicate an inflamed environment and treated with free Curcumin and Curc-SPNs. Note that the stimulation of macrophages with A β fibrils was consider as a preliminary model of neuro-inflammation in AD (46). Results demonstrated a significant efficacy of Curc-SPNs in modulating the production of pro-inflammatory cytokines, namely IL-1 β , IL-6, and TNF- α . Importantly, no changes in

gene expression (in particular for IL-6 and TNF- α) (47) was observed upon the incubation of macrophages with empty SPNs. This additional control indirectly confirm the absence of endotoxin or of any unintentional contamination with minute amount of LPS, which would have induced a powerful inflammatory response (48). Interestingly, at the considered concentrations, the pro-inflammatory effect of LPS was always stronger than that associated with fibrillar A β incubation. Finally, no cytotoxic effect was observed after the incubation of the cells with the vehicle *per se*, as well as the ability of the system to preserve the structure and the function of Curcumin, after being loaded into the polymeric matrix. Altogether these findings demonstrate that spherical polymeric nanoconstructs can efficiently target macrophages and alleviate inflammation by the specific, intracellular delivery of Curcumin. This approach holds potential in the mitigation of inflammation in AD. However, future works should progress along two parallel paths. On the one hand, more sophisticated *in vitro* models will have to be considered where primary microglia and neurons are co-cultured and monitored over time during treatment for assessing cytokine production as well as neuronal activity. On the other hand, the role of tissue inflammation on the blood

brain barrier permeability to nanoparticles should be elucidated using imaging and different pre-clinical models of AD.

AUTHOR CONTRIBUTIONS

AA: synthesis and chemico-physical and biological characterization of the spherical polymeric nanoconstructs (SPNs); RP: performed confocal microscopy and FACS analyses; AP: synthesis and chemico-physical and biological characterization of the discoidal polymeric nanoparticles (DPNs); AL and AC: helped with the synthesis and characterization of SPNs; DM: helped with the synthesis and characterization of SPNs and manuscript writing; PD: coordinated the work and manuscript writing. Results were analyzed and discussed by all authors.

ACKNOWLEDGMENTS

This work was partially supported by the European Research Council, under the European Union's Seventh Framework Programme (FP7/2007-2013)/ERC grant agreement no. 616695 and the AIRC (Italian Association for Cancer Research) under the individual investigator grant no. 17664.

REFERENCES

- Medzhitov R. Origin and physiological roles of inflammation. *Nature* (2008) 454:428–35. doi:10.1038/nature07201
- Rocha VZ, Libby P. Obesity, inflammation, and atherosclerosis. *Nat Rev Cardiol* (2009) 6:399–409. doi:10.1038/nrcardio.2009.55
- Gajewski TE, Schreiber H, Fu YX. Innate and adaptive immune cells in the tumor microenvironment. *Nat Immunol* (2013) 14:1014–22. doi:10.1038/ni.2703
- Hotamisligil GS. Inflammation and metabolic disorders. *Nature* (2006) 444:860–7. doi:10.1038/nature05485
- Heppner FL, Ransohoff RM, Becher B. Immune attack: the role of inflammation in Alzheimer disease. *Nat Rev Neurosci* (2015) 16:358–72. doi:10.1038/nrn3880
- Akiyama H, Barger S, Barnum S, Bradt B, Bauer J, Cole GM, et al. Inflammation and Alzheimer's disease. *Neurobiol Aging* (2000) 21:383–421. doi:10.1016/S0197-4580(00)00124-X
- Mandrekar-Colucci S, Landreth GE. Microglia and inflammation in Alzheimer's disease. *CNS Neurol Disord Drug Targets* (2010) 9:156–67. doi:10.2174/187152710791012071
- Peer D, Karp JM, Hong S, Farokhzad OC, Margalit R, Langer R. Nanocarriers as an emerging platform for cancer therapy. *Nat Nanotechnol* (2007) 2:751–60. doi:10.1038/nnano.2007.387
- Min Y, Caster JM, Eblan MJ, Wang AZ. Clinical translation of nanomedicine. *Chem Rev* (2015) 115:11147–90. doi:10.1021/acs.chemrev.5b00116
- Champion JA, Katare YK, Mitragotri S. Particle shape: a new design parameter for micro- and nanoscale drug delivery carriers. *J Control Release* (2007) 121:3–9. doi:10.1016/j.jconrel.2007.03.022
- Decuzzi P, Pasqualini R, Arap W, Ferrari M. Intravascular delivery of particulate systems: does geometry really matter? *Pharm Res* (2009) 26:235–43. doi:10.1007/s11095-008-9697-x
- Gratton SE, Ropp PA, Pohlhaus PD, Luft JC, Madden VJ, Napier ME, et al. The effect of particle design on cellular internalization pathways. *Proc Natl Acad Sci U S A* (2008) 105:11613–8. doi:10.1073/pnas.0801763105
- Merkel TJ, Chen K, Jones SW, Pandya AA, Tian S, Napier ME, et al. The effect of particle size on the biodistribution of low-modulus hydrogel PRINT particles. *J Control Release* (2012) 162:37–44. doi:10.1016/j.jconrel.2012.06.009
- Key J, Aryal S, Gentile F, Ananta JS, Zhong M, Landis MD, et al. Engineering discoidal polymeric nanoconstructs with enhanced magneto-optical properties for tumor imaging. *Biomaterials* (2013) 34:5402–10. doi:10.1016/j.biomaterials.2013.03.078
- Key J, Palange AL, Gentile F, Aryal S, Stigliano C, Di Mascolo D, et al. Soft discoidal polymeric nanoconstructs resist macrophage uptake and enhance vascular targeting in tumors. *ACS Nano* (2015) 9:11628–41. doi:10.1021/acsnano.5b04866
- Stigliano C, Key J, Ramirez M, Aryal S, Decuzzi P. Radiolabeled polymeric nanoconstructs loaded with docetaxel and curcumin for cancer combinatorial therapy and nuclear imaging. *Adv Funct Mater* (2015) 25:3371–9. doi:10.1002/adfm.201500627
- Lee A, Di Mascolo D, Francardi M, Piccardi F, Bandiera T, Decuzzi P. Spherical polymeric nanoconstructs for combined chemotherapeutic and anti-inflammatory therapies. *Nanomedicine* (2016) 12:2139–47. doi:10.1016/j.nano.2016.05.012
- Palange AL, Di Mascolo D, Carallo C, Gnasso A, Decuzzi P. Lipid-polymer nanoparticles encapsulating curcumin for modulating the vascular deposition of breast cancer cells. *Nanomedicine* (2014) 10:e991–1002. doi:10.1016/j.nano.2014.02.004
- Zhang L, Chan JM, Gu FX, Rhee JW, Wang AZ, Radovic-Moreno AF, et al. Self-assembled lipid-polymer hybrid nanoparticles: a robust drug delivery platform. *ACS Nano* (2008) 2:1696–702. doi:10.1021/nn800275r
- Murray PJ, Wynn TA. Protective and pathogenic functions of macrophage subsets. *Nat Rev Immunol* (2011) 11:723–37. doi:10.1038/nri3073
- El Khoury J, Hickman SE, Thomas CA, Cao L, Silverstein SC, Loike JD. Scavenger receptor-mediated adhesion of microglia to β -amyloid fibrils. *Nature* (1996) 382:716–9. doi:10.1038/382716a0
- Bamberger ME, Harris ME, McDonald DR, Husemann J, Landreth GE. A cell surface receptor complex for fibrillar β -amyloid mediates microglial activation. *J Neurosci* (2003) 23:2665–74.
- Paresce DM, Ghosh RN, Maxfield FR. Microglial cells internalize aggregates of the Alzheimer's disease amyloid β -protein via a scavenger receptor. *Neuron* (1996) 17:553–65. doi:10.1016/S0896-6273(00)80187-7
- Stewart CR, Stuart LM, Wilkinson K, van Gils JM, Deng J, Halle A, et al. CD36 ligands promote sterile inflammation through assembly of a toll-like receptor 4 and 6 heterodimer. *Nat Immunol* (2010) 11:155–61. doi:10.1038/ni.1836
- Sheedy FJ, Grebe A, Rayner KJ, Kalantari P, Ramkhalawon B, Carpenter SB, et al. CD36 coordinates NLRP3 inflammasome activation by facilitating intracellular nucleation of soluble ligands into particulate ligands in sterile inflammation. *Nat Immunol* (2013) 14:812–20. doi:10.1038/ni.2639

26. Koenigsnecht J, Landreth G. Microglial phagocytosis of fibrillar β -amyloid through a β 1 integrin-dependent mechanism. *J Neurosci* (2004) 24:9838–46. doi:10.1523/JNEUROSCI.2557-04.2004
27. Fassbender K, Walter S, Kühl S, Landmann R, Ishii K, Bertsch T, et al. The LPS receptor (CD14) links innate immunity with Alzheimer's disease. *FASEB J* (2004) 18:203–5. doi:10.1096/fj.03-0364fj
28. El Khoury JB, Moore KJ, Means TK, Leung J, Terada K, Toft M, et al. CD36 mediates the innate host response to β -amyloid. *J Exp Med* (2003) 197:1657–66. doi:10.1084/jem.20021546
29. Griffin WS, Stanley LC, Ling C, White L, MacLeod V, Perrot LJ, et al. Brain interleukin 1 and S-100 immunoreactivity are elevated in Down syndrome and Alzheimer disease. *Proc Natl Acad Sci U S A* (1989) 86:7611–5. doi:10.1073/pnas.86.19.7611
30. Patel NS, Paris D, Mathura V, Quadros AN, Crawford FC, Mullan MJ. Inflammatory cytokine levels correlate with amyloid load in transgenic mouse models of Alzheimer's disease. *J Neuroinflammation* (2005) 2:1. doi:10.1186/1742-2094-2-9
31. Vom Berg J, Prokop S, Miller KR, Obst J, Kälin RE, Lopategui-Cabezas I, et al. Inhibition of IL-12/IL-23 signaling reduces Alzheimer's disease-like pathology and cognitive decline. *Nat Med* (2012) 18:1812–9. doi:10.1038/nm.2965
32. Fillit H, Ding WH, Buee L, Kalman J, Altstiel L, Lawlor B, et al. Elevated circulating tumor necrosis factor levels in Alzheimer's disease. *Neurosci Lett* (1991) 129:318–20. doi:10.1016/0304-3940(91)90490-K
33. Mawuenyega KG, Sigurdson W, Ovod V, Munsell L, Kasten T, Morris JC, et al. Decreased clearance of CNS β -amyloid in Alzheimer's disease. *Science* (2010) 330:1774–1774. doi:10.1126/science.1197623
34. Kumar S, Anselmo AC, Banerjee A, Zakrewsky M, Mitragotri S. Shape and size-dependent immune response to antigen-carrying nanoparticles. *J Control Release* (2015) 220:141–8. doi:10.1016/j.jconrel.2015.09.069
35. Anselmo AC, Zhang M, Kumar S, Vogus DR, Menegatti S, Helgeson ME, et al. Elasticity of nanoparticles influences their blood circulation, phagocytosis, endocytosis, and targeting. *ACS Nano* (2015) 9:3169–77. doi:10.1021/acsnano.5b00147
36. Lunov O, Syrovets T, Loos C, Beil J, Delacher M, Tron K, et al. Differential uptake of functionalized polystyrene nanoparticles by human macrophages and a monocytic cell line. *ACS Nano* (2011) 5:1657–69. doi:10.1021/nn2000756
37. Dos Santos T, Varela J, Lynch I, Salvati A, Dawson KA. Quantitative assessment of the comparative nanoparticle-uptake efficiency of a range of cell lines. *Small* (2011) 7:3341–9. doi:10.1002/smll.201101076
38. Di Mascolo D, J Lyon C, Aryal S, Ramirez MR, Wang J, Candeloro P, et al. Rosiglitazone-loaded nanospheres for modulating macrophage-specific inflammation in obesity. *J Control Release* (2013) 170:460–8. doi:10.1016/j.jconrel.2013.06.012
39. Stigliano C, Ramirez MR, Singh JV, Aryal S, Key J, Blanco E, et al. Methotrexate-loaded hybrid nanoconstructs target vascular lesions and inhibit atherosclerosis progression in ApoE $^{-/-}$ mice. *Adv Healthcare Mater* (2017) 6:1601286. doi:10.1002/adhm.201601286
40. Lee A, Mei CD, Fereira M, Marotta R, Yoon HY, Kim K, et al. Dexamethasone-loaded polymeric nanoconstructs for monitoring and treating inflammatory bowel disease. *Theranostic* (2017) 7(15):3654. doi:10.7150/thno.18183
41. Wilken R, Veena MS, Wang MB, Srivatsan ES. Curcumin: a review of anti-cancer properties and therapeutic activity in head and neck squamous cell carcinoma. *Mol Cancer* (2011) 10:12. doi:10.1186/1476-4598-10-12
42. Shehzad A, Rehman G, Lee YS. Curcumin in inflammatory diseases. *Biofactors* (2013) 39:69–77. doi:10.1002/biof.1066
43. Ireson C, Orr S, Jones DJ, Verschoyle R, Lim CK, Luo JL, et al. Characterization of metabolites of the chemopreventive agent curcumin in human and rat hepatocytes and in the rat in vivo, and evaluation of their ability to inhibit phorbol ester-induced prostaglandin E2 production. *Cancer Res* (2001) 61:1058–64.
44. Sharma RA, McLelland HR, Hill KA, Ireson CR, Euden SA, Manson MM, et al. Pharmacodynamic and pharmacokinetic study of oral curcuma extract in patients with colorectal cancer. *Clin Cancer Res* (2001) 7:1894–900.
45. Dhillon N, Aggarwal BB, Newman RA, Wolff RA, Kunnumakkara AB, Abbruzzese JL, et al. Phase II trial of curcumin in patients with advanced pancreatic cancer. *Clin Cancer Res* (2008) 14:4491–9. doi:10.1158/1078-0432.CCR-08-0024
46. Smits HA, van Beelen AJ, de Vos NM, Rijmsus A, van der Bruggen T, Verhoef J, et al. Activation of human macrophages by amyloid- β is attenuated by astrocytes. *J Immunol* (2001) 166:6869–76. doi:10.4049/jimmunol.166.11.6869
47. Schwarz H, Gornicec J, Neuper T, Parigiani MA, Wallner M, Duschl A, et al. Biological activity of masked endotoxin. *Sci Rep* (2017) 7:44750. doi:10.1038/srep44750
48. Boraschi D, Italiani P, Palomba R, Decuzzi P, Duschl A, Fadeel B, et al. Nanoparticles and innate immunity: new perspectives on host defence. *Semin Immunol* (2017). doi:10.1016/j.smim.2017.08.013

Conflict of Interest Statement: The authors declare that the research was conducted in the absence of any commercial or financial relationships that could be construed as a potential conflict of interest.

Copyright © 2017 Ameruoso, Palomba, Palange, Cervadoro, Lee, Di Mascolo and Decuzzi. This is an open-access article distributed under the terms of the Creative Commons Attribution License (CC BY). The use, distribution or reproduction in other forums is permitted, provided the original author(s) or licensor are credited and that the original publication in this journal is cited, in accordance with accepted academic practice. No use, distribution or reproduction is permitted which does not comply with these terms.